SIAM J. APPL. MATH.
Vol. 78, No. 3, pp. 1754–1777

ACTIN-MYOSIN FORCE GENERATION AND SYMMETRY BREAKING IN THE MODEL CONTRACTILE FIBER*

BEN FOGELSON† AND ALEX MOGILNER‡

Abstract. Myosin-powered force generation in nonmuscle cells underlies many cell biological processes and is based on contraction of random actin arrays. One of the most prominent examples of such arrays is a contractile fiber—a one-dimensional actin-myosin fiber with focal adhesions at its ends. We explore an active gel model widely used in theoretical biophysics with effective viscous dashpots at the ends of the actin-myosin gel strip as a model for such a fiber. Scaling analysis reveals that three length scales characterize the behavior of the model, which consists of two PDEs describing force balance and myosin transport in the fiber. We use singular perturbation analysis and numerical simulations to investigate how the myosin distribution, actin flow, and contractile force generated by the fiber depend on model parameters and fiber length. The model predicts that the contractile force either increases, with or without saturation, with fiber length, or reaches a maximum at certain length and then decreases in longer fibers, depending on parameters. The model also predicts a nontrivial symmetry-breaking mechanism: in long fibers with strong focal adhesions at the ends, the myosin distribution is not uniform but peak-like, and this peak can aggregate to one of the fiber's ends. We discuss the model's implication for mechanobiology of nonmuscle cells.

Key words. actin, myosin, force, contraction, symmetry breaking, stress fiber

AMS subject classifications. 92B05, 92C05, 92C10, 92C37, 35Q92

DOI. 10.1137/17M1112261

1. Introduction.

Force generation is one of the most fundamental actions of a cell. Prominent examples include cell motility [12], cell division [12], and muscle contraction [51]. A major component of the cellular force-production machinery is the actin-myosin system, which at its core consists of a scaffold of actin filaments upon which myosin motors act to produce contractile stress [49, 54]. Actin-myosin contraction is fundamental to muscular force production and, in nonmuscle cells, for producing force in one-dimensional structures such as dynamic stress fibers (SFs) [49] and cytokinetic rings [35]; two-dimensional structures such as lamellipodia [3] and cell cortices [10]; and three-dimensional cytoskeletal networks in migrating cells [13]. Important parts of this system are crosslinking proteins [29, 46, 53] that transiently bind actin filaments together, creating effective internal friction and, in nonmuscle cells, focal adhesion complexes that transduce force from actin-myosin arrays to the extracellular matrix [18, 21].

In this paper, we focus on one-dimensional contractile networks of actin, myosin, and crosslinking proteins in nonmuscle cells. The most prominent example of such a network that comes to mind is the SF, a one-dimensional actomyosin bundle that extends between focal adhesions (FAs) and is found in many types of cells [49]. Much

*Received by the editors January 19, 2017; accepted for publication (in revised form) April 24, 2018; published electronically June 19, 2018.
http://www.siam.org/journals/siap/78-3/M111226.html
Funding: This material is based upon work supported by the National Science Foundation Graduate Research Fellowship Program under NSF grant DGE1342536. Any opinions, findings, and conclusions or recommendations expressed in this material are those of the authors and do not necessarily reflect the views of the National Science Foundation.

†Department of Mathematics, University of Utah, Salt Lake City, UT 84112 (ben@math.utah.edu, http://math.utah.edu/~ben).
‡Courant Institute of Mathematical Sciences, New York University, New York, NY 10012 (mogilner@cims.nyu.edu, http://cims.nyu.edu/~mogilner).

experimental research has been devoted to the assembly and dynamics of SFs, but the molecular mechanisms underlying their assembly are still largely unknown [49]. Similarly, a number of studies have experimentally measured contractile forces generated by SFs in cells [11, 14, 25, 26] and in vitro [15]. It was found that the generated force increases with the length of the contractile fiber in vitro [47].

A number of modeling papers have been devoted to force-dependent assembly of SFs [5, 17, 43, 44, 52]. A few models specifically address the question of how much force the SFs generate by considering muscle-like units connected in series, together with viscoelastic elements [44]. There was also an active investigation of microscopic mechanisms of force generation in random actin-myosin-crosslinker arrays [28, 32].

In this paper, we investigate a one-dimensional continuous "active gel" model widely used in soft matter physics and biophysics [6, 8, 24, 38]. In the remainder of the paper, we call the subject of the investigation a contractile fiber (CF) and emphasize that we model an idealized macroscopic CF, in the sense that we do not deal with the precise mechanism of force generation by individual actin filaments and myosin motors. In the discussion (section 7), we address the issue of the model's applicability to specific biological structures, such as SFs, in vitro contractile bundles, cytokinetic contractile rings, and lamellipodial networks.

The model consists of two PDEs: one describing myosin transport and another the balance of active contractile force with the passive forces of crosslinking and adhesion in the fiber. The novel parts of the model are the mechanical boundary conditions at the FAs at the CF ends. We use perturbation theory analysis and numerical simulations to find highly nontrivial distributions of myosin and deformations of the CF and the force generated by the CF as a function of its length.

Besides force generation, the contractile networks also play a critical role in cell polarization [37]. Polarization is the process by which a cell breaks symmetry and transitions from a symmetric to an asymmetric configuration, in terms of its distribution of actin, myosin, and crosslinking elements, as well as its mechanical properties. Such symmetry breaking is a necessary step in motility initiation: before a cell can move, it must develop a defined front and rear [2]. It was shown in [2, 38] that such symmetry breaks can be purely mechanical, based on contraction and redistribution of myosin in the active gel, but physical movement of the whole cell was an essential part of the phenomenon. In this paper, we report the finding that a mechanical symmetry break can occur in stationary CFs and come up with a physical explanation for this self-organizing asymmetry.

2. Mathematical model of actin-myosin CF mechanics. Our model consists of two equations: a force balance equation and a transport equation. The force balance equation has the form

$$\frac{\partial}{\partial x}\left(\mu\frac{\partial v}{\partial x}+km\right)=\xi v,\quad -\tfrac{L}{2}<x<\tfrac{L}{2}, \tag{2.1}$$

$$\mu\frac{\partial v}{\partial x}+km=\zeta_l v\Big|_{x=-\frac{L}{2}},\quad \mu\frac{\partial v}{\partial x}+km=-\zeta_r v\Big|_{x=\frac{L}{2}}. \tag{2.2}$$

We assume a constant fiber length of L and define two dependent variables for $-\frac{L}{2}<x<\frac{L}{2}$: the velocity of the actin-myosin gel $v(x,t)$ and the myosin density $m(x,t)$ for position x and time t. The term in parentheses on the left describes the one-dimensional sum of two stresses: the effective viscous stress that results from transient crosslinks between actin filaments in the CF and the active stress due to myosin contraction. This latter stress is assumed to be proportional to the myosin density.

TABLE 2.1
Variables and parameters in the dimensional SF model.

Notation	Meaning	Units
L	length of stress fiber	μm
k	myosin motor contraction strength	$\frac{\text{pN} \times \mu\text{m}}{\text{myosin}}$
μ	stress fiber internal viscosity coefficient	$\text{pN} \times \text{s}$
ξ	cortex drag coefficient	$\frac{\text{pN}}{\mu\text{m}\,\text{s}^{-1}} \times \frac{1}{\mu\text{m}}$
ζ_l, ζ_r	adhesion friction coefficients	$\frac{\text{pN}}{\mu\text{m}\,\text{s}^{-1}}$
D	effective myosin diffusion coefficient	$\mu\text{m}^2\,\text{s}^{-1}$
x	location along stress fiber	μm
t	time	s
$v(x,t)$	actin-myosin gel velocity	$\mu\text{m}\,\text{s}^{-1}$
$m(x,t)$	myosin linear density	myosin/μm

Here k is the proportionality constant giving the mechanical strength per unit myosin and μ is the constant effective actin-myosin gel viscosity. We balance the divergence of these two stresses against the frictional force per unit length that results from transient crosslinking of filaments in the fiber with filaments in the neighboring (and assumed stationary) actin cortex. Following a number of previous models, we assume that this friction is effectively viscous, proportional to the gel velocity; ξ is the constant of proportionality. Table 2.1 summarizes the model variables and parameters.

We derive the boundary conditions (2.2) by balancing the stress at the left and right SF endpoints with the effective friction force between the flowing actin-myosin gel and adhesive proteins of the FAs at the SF ends. We assume that this friction is linear and viscous, with ζ_l and ζ_r as the strengths of friction of the left and right FAs, respectively.

Together, these mechanical equations prescribe the local actin velocity $v(x,t)$ for a given linear density $m(x,t)$ of myosin. To close the system, we need an equation for this myosin density. Following previous modeling, we assume that myosin molecules are bound to the actin gel most of the time and drift with it. Molecules frequently unbind from actin, diffuse in the cytoplasm, and rapidly rebind. In the limit of fast binding and unbinding kinetics, the total linear myosin density can be described with the drift-diffusion equation

$$\frac{\partial m}{\partial t} + \frac{\partial}{\partial x}\Big(vm\Big) = D\frac{\partial^2 m}{\partial x^2}, \quad -\tfrac{L}{2} < x < \tfrac{L}{2}, \tag{2.3}$$

$$vm = D\frac{\partial m}{\partial x}\Big|_{x=\pm\frac{L}{2}}, \tag{2.4}$$

where D is the effective diffusion coefficient in the fast kinetic limit and where the natural boundary conditions in (2.4) mean that there is no flux of myosin out of the endpoints of the CF. There are other reasonable ways to model myosin dynamics. In section SM1 of the supplementary materials, linked from the main article webpage, we discuss two alternate models: the full kinetic model with bound and unbound myosin populations and a model with a constant reservoir of cytoplasmic myosin. There we show that each of these alternatives gives qualitatively similar results to the drift-diffusion model of (2.3) and (2.4).

We are interested in using this model to compute the traction stress exerted by the fiber on the underlying substrate, since traction stress is the important mechanical

output for the cell and is what can be measured in experiments. To find this, we must compute the force exerted by the CF on its left and right ends. If the only stresses acting on the adhesions were those produced by the fiber, then from (2.2) the stresses at the left and right would be $\zeta_l v(-\frac{L}{2},t)$ and $\zeta_r v(\frac{L}{2},t)$, respectively. In general, however, our model does not guarantee that $\zeta_l v(-\frac{L}{2},t)$ and $\zeta_r v(\frac{L}{2},t)$ are equal and opposite. In particular, we expect that for nonzero ξ, drag between the SF and the actin cortex will likely lead to different stresses at the two endpoints. To correctly compute the traction stress at the two endpoints, we need to take into account how drag by the CF on the cortex generates additional stresses acting on the two FAs.

The cortex is a dense, branched network of actin filaments. Because of this mesh-like structure, individual filaments in the cortex are far less motile than filaments in the fiber. With this in mind, we model the cortex as a solid, nondeformable structure. This means that we can write the net drag force exerted by CF on the cortex as

$$F_{\text{drag}} = \xi \int_{-\frac{L}{2}}^{\frac{L}{2}} v(x,t)\, dx. \tag{2.5}$$

This force will be positive if the solid cortex is being dragged to the right and negative if it is being dragged to the left. Since cells typically build FAs to tether actin that is being pulled away from the adhesion, we assume that for $F_{\text{drag}} > 0$ the entire net drag force is applied to the left adhesion, and similarly for $F_{\text{drag}} < 0$. Under this assumption, we can define the traction force as

$$F_{\text{traction}} = \zeta_l v\big(-\tfrac{L}{2},t\big) + \max\big(F_{\text{drag}},0\big) = -\zeta_r v\big(\tfrac{L}{2},t\big) + \min\big(F_{\text{drag}},0\big). \tag{2.6}$$

We can reduce the number of parameters in the model by rescaling (2.1)–(2.4). The natural choices for length scale and myosin density are the CF length L and the conserved average myosin density $\overline{m}$, respectively. By balancing the viscous and myosin stresses in the force balance equation, we obtain the characteristic velocity scale, $k\overline{m}L/\mu$. Dividing the length scale by the velocity scale, we get the time scale, $\mu/k\overline{m}$. Introducing nondimensional variables by dividing the dimensional ones by the chosen scales, we arrive at the nondimensional system, where we keep the same notation for the nondimensional variables:

$$\frac{\partial}{\partial x}\left(\frac{\partial v}{\partial x} + m\right) = \alpha^2 v, \quad -\tfrac{1}{2} < x < \tfrac{1}{2}, \tag{2.7}$$

$$\frac{\partial v}{\partial x} + m = \beta_l v\Big|_{x=-\frac{1}{2}}, \quad \frac{\partial v}{\partial x} + m = -\beta_r v\Big|_{x=\frac{1}{2}}, \tag{2.8}$$

$$\frac{\partial m}{\partial t} + \frac{\partial}{\partial x}\Big(vm\Big) = \gamma \frac{\partial^2 m}{\partial x^2}, \quad -\tfrac{1}{2} < x < \tfrac{1}{2}, \tag{2.9}$$

$$vm = \gamma \frac{\partial m}{\partial x}\Big|_{x=\pm\frac{1}{2}}. \tag{2.10}$$

The system behavior depends on four nondimensional parameter combinations:

$$\alpha = \sqrt{\frac{\xi}{\mu}}L, \quad \beta_{l,r} = \frac{L\zeta_{l,r}}{\mu}, \quad \text{and} \quad \gamma = \frac{D\mu}{k\overline{m}L^2}. \tag{2.11}$$

Parameter α^2 serves as the nondimensionalized cortex drag coefficient, while parameters $\beta_{l,r}$ are the nondimensional FA friction coefficients at the left and right, respectively. Parameter γ is the nondimensional diffusion coefficient. Note that γ can also

be thought of as one over the Péclet number from classical fluid mechanics, so we can interpret γ as the rate of diffusive myosin transport over the rate of advective myosin transport.

The profound meaning of these nondimensional parameter combinations is that they introduce three fundamental length scales and that competition between these length scales completely governs the model behavior. For $\beta_l = \beta_r = \beta$ we can write $\alpha = L/L_{\text{drag}}$, $\beta = L/L_{\text{friction}}$, and $\gamma = (L_{\text{diffusion}}/L)^2$, so the system can be characterized by the ratios of the CF length to the length scales L_{drag}, L_{friction}, and $L_{\text{diffusion}}$. $L_{\text{drag}} = \sqrt{\mu/\xi}$ determines the characteristic length over which the CF can transmit forces through the interior before substantial drag-induced decay. Similarly, $L_{\text{friction}} = \mu/\zeta$ is the characteristic length over which viscosity can transmit forces from inside the fiber to a focal adhesion. Finally, $L_{\text{diffusion}} = \sqrt{D\mu/k\overline{m}}$ is the characteristic distance by which myosin diffuses over the characteristic time scale. In what follows, we examine nonrigorously, semiquantitatively, the system's behavior predicted by the model in two regimes: $L \ll L_{\text{diffusion}}$ and $L \gg L_{\text{diffusion}}$. We investigate how this behavior depends on the length scales L_{drag} and L_{friction}. Then we confirm our gained intuition with perturbation analysis and numerical simulations.

3. Model predictions in the limit of fast diffusion. We start with the limit $\gamma \to \infty$, which corresponds to a CF so short that diffusion spreads myosin almost uniformly across the CF. Indeed, in this limit, a zeroth-order approximation in a regular perturbation of the myosin equations (2.9) and (2.10) gives the simple solution

$$m(x,t) = 1. \tag{3.1}$$

(In dimensional units, $m(x,t) = \overline{m}$.) From (3.1), the velocity equations (2.7) and (2.8) simplify to

$$\frac{\partial^2 v}{\partial x^2} = \alpha^2 v, \quad -\tfrac{1}{2} < x < \tfrac{1}{2}, \tag{3.2}$$

$$\frac{\partial v}{\partial x} + 1 = \beta_l v\Big|_{x=-\frac{1}{2}}, \quad \frac{\partial v}{\partial x} + 1 = -\beta_r v\Big|_{x=\frac{1}{2}}. \tag{3.3}$$

These equations have the explicit solution

$$v(x,t) = -\frac{2\alpha \sinh\left(\frac{\alpha}{2}\right)\sinh(\alpha x) + \beta_l \sinh\left(\alpha(x+\frac{1}{2})\right) + \beta_r \sinh\left(\alpha(x-\frac{1}{2})\right)}{\alpha(\beta_l+\beta_r)\cosh\alpha + (\alpha^2+\beta_l\beta_r)\sinh\alpha}. \tag{3.4}$$

There is a centripetal actin-myosin gel flow, with velocities that are positive at the left and negative at the right (such flows are depicted in Figure 3.1). Such a flow profile makes intuitive sense—since myosin motors are contractile, they should pull the gel inward.

From this expression for the actin flow, we can compute the traction stress F_{traction} that the cell exerts on the substrate. We derived the expression for this stress in (2.5) and (2.6) in terms of dimensional variables. In nondimensional form, we write it as

$$f_{\text{drag}} = \frac{F_{\text{drag}}}{k\overline{m}} = \alpha^2 \int_{-\frac{1}{2}}^{\frac{1}{2}} v(x,t)\, dx, \tag{3.5}$$

$$f_{\text{traction}} = \frac{F_{\text{traction}}}{k\overline{m}} = \beta_l v\big(-\tfrac{1}{2},t\big) + \max\big(f_{\text{drag}},0\big) = -\beta_r v\big(\tfrac{1}{2},t\big) + \min\big(f_{\text{drag}},0\big). \tag{3.6}$$

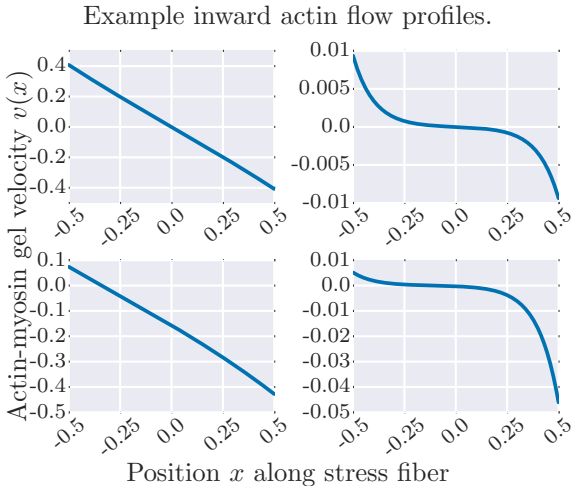

FIG. 3.1. *Characteristic actin flow profiles from* (3.4) *for several values of* α, β_l, *and* β_r. *For any parameter values, actin flows inward from both the left and the right edges of the fiber, as we expect for a contraction-driven flow. Top left:* $\alpha = 1$, $\beta_l = 1$, $\beta_r = 1$. *Top right:* $\alpha = 10$, $\beta_l = 1$, $\beta_r = 1$. *Bottom right:* $\alpha = 1$, $\beta_l = 10$, $\beta_r = 1$. *Bottom left:* $\alpha = 10$, $\beta_l = 10$, $\beta_r = 1$.

First, we compute f_{traction} for the special case $\beta_l = \beta_r = \beta$, when the two focal adhesions are equally strong. In this case, symmetry requires that $f_{\text{drag}} = 0$, which simplifies f_{traction} to

$$f_{\text{traction}} = \beta v\left(-\tfrac{1}{2}, t\right) = -\beta v\left(\tfrac{1}{2}, t\right) \tag{3.7}$$

$$= \frac{\beta}{\beta + \alpha \coth \frac{\alpha}{2}}. \tag{3.8}$$

To see how the traction forces scales with CF length, we rewrite f_{traction} with $\alpha = L/L_{\text{drag}}$ and $\beta = L/L_{\text{friction}}$:

$$f_{\text{traction}} = \frac{L_{\text{drag}}}{L_{\text{drag}} + L_{\text{friction}} \coth \frac{L}{2L_{\text{drag}}}}. \tag{3.9}$$

For small L ($L \ll L_{\text{drag}}$), we can expand (3.9) to

$$f_{\text{traction}} = \frac{L}{2L_{\text{friction}}} + \mathcal{O}(L^2), \tag{3.10}$$

which implies that for a sufficiently short fiber, the cell exerts a force on the substrate that grows linearly with fiber length. At the opposite extreme, when L is large (compared to L_{drag}, as far as $L_{\text{drag}} \ll L_{\text{diffusion}}$), we obtain the limit

$$f_{\text{traction}} \to \frac{L_{\text{drag}}}{L_{\text{drag}} + L_{\text{friction}}}. \tag{3.11}$$

The case $\beta_l \neq \beta_r$ makes for more complicated intermediate calculations but produces qualitatively similar results. When $\beta_l < \beta_r$, for small L we compute

$$f_{\text{traction}} = \frac{L}{L_{\text{friction},l} + L_{\text{friction},r}} + \mathcal{O}(L^2), \tag{3.12}$$

while for large L we find that

$$f_{\text{traction}} \to \frac{L_{\text{drag}}}{L_{\text{drag}} + L_{\text{friction},r}}. \tag{3.13}$$

Thus, (3.12) and (3.13) exhibit the same qualitative force scaling behavior as (3.10) and (3.11): linear at low L and constant at high L.

The physical interpretation of these results is as follows. Myosin motors distributed over the CF length work in series: one can imagine people standing in line holding hands and pulling each other in. The maximal stress that can be developed in such a chain is equal to the stress of any unit of this chain ($k\overline{m}$ in dimensional units). If the CF is long enough (but still shorter than $L_{\text{diffusion}}$), so that the myosin contractile stress is not dampened significantly by the actin viscosity, and if the cortex drag is negligible, then this maximal stress is all transduced to the FAs, in agreement with (3.11). In this case, the gel velocity profile is linear. Basically, if the CF is long enough, the gradient of the velocity across the CF is shallow enough to render actin viscosity negligible. However, if the cortex drag is not negligible, the gel velocity profile changes: velocity at the CF center becomes almost zero, and the centripetal velocity only becomes significant near the edges of the fiber. In this case, cortex drag dampens the maximal possible traction force by the factor $L_{\text{drag}}/(L_{\text{drag}} + L_{\text{friction}})$. When the CF becomes very short (compared to L_{friction}), the gradient of the velocity across the CF that is needed to create significant centripetal flow at the FAs becomes so large that the actin viscosity decreases the myosin power output: effectively, myosin works mostly against internal viscous friction. In this limit, force is proportional to CF length.

4. Model predictions in the limit of slow diffusion. In the slow diffusion limit where the CF is long compared to $L_{\text{diffusion}}$, $\gamma \to 0$ in (2.3) and (2.9). This is a singular perturbation problem and thus more mathematically challenging than the $\gamma \to \infty$ limit. We defer the full analysis of the singular perturbation problem to section 6. For now, we study this limit by considering a physically motivated ansatz about myosin dynamics. This will provide us with important new intuition, which we will extend to the full model using numerical simulations and then confirm with singular perturbation analysis.

We use the following physical reasoning: in our model, myosin drifts with the local velocity v. This velocity is itself influenced by myosin, since motors exert contractile force on the gel. As we saw, this force produces an inward flow, which pulls myosin motors towards one another. This suggests that myosin will coalesce into a single cluster. With low diffusion, this cluster may be quite localized. Based on this prediction, we choose to approximate the myosin density in the limit as $\gamma \to 0$ as an infinitely sharp peak, replacing $m(x,t)$ with a Dirac δ function. In general, this δ function may be located at any x and the location might change with time. For now, however, we assume that the adhesions at the left and right are equal, $\beta_l = \beta_r = \beta$, and from symmetry that the location of the peak is fixed at the CF center, $x = 0$.

Under these assumptions, our model equations become

$$\frac{\partial^2 v}{\partial x^2} - \alpha^2 v = -\frac{\partial \delta_0}{\partial x}, \quad -\tfrac{1}{2} < x < \tfrac{1}{2}, \tag{4.1}$$

$$\frac{\partial v}{\partial x} = \beta v\Big|_{x=-\frac{1}{2}}, \quad \frac{\partial v}{\partial x} = -\beta v\Big|_{x=\frac{1}{2}}. \tag{4.2}$$

Equations (4.1) and (4.2) are an inhomogeneous linear boundary value problem, so we can solve for v by finding a particular solution v_p to (4.1) as well as the general solution to the homogeneous problem. Using a Fourier transform, we find that

$$v_p(x) = \frac{e^{\alpha x}H(-x) - e^{-\alpha x}H(x)}{2}, \tag{4.3}$$

where H is the Heaviside function. We easily solve the homogeneous problem to give the general solution

$$v_0 = c_1 \sinh \alpha x + c_2 \cosh \alpha x. \tag{4.4}$$

To compute c_1 and c_2, we set $v = v_0 + v_p$ and use the boundary conditions from (4.2). From this we find that the solution to the full inhomogeneous problem is

$$v(x) = \frac{\beta - \alpha}{\alpha - \beta + e^{\alpha}(\alpha + \beta)} \sinh \alpha x + \frac{e^{\alpha x}H(-x) - e^{-\alpha x}H(x)}{2}. \tag{4.5}$$

Computing the traction force from (4.5), we get

$$f_{\text{traction}} = \frac{\alpha\beta}{2\alpha \cosh \frac{\alpha}{2} + 2\beta \sinh \frac{\alpha}{2}} = \frac{L}{2L_{\text{friction}} \cosh \frac{L}{2L_{\text{drag}}} + 2L_{\text{drag}} \sinh \frac{L}{2L_{\text{drag}}}}. \tag{4.6}$$

For small L, this expands to

$$f_{\text{traction}} = \frac{L}{2L_{\text{friction}}} + \mathcal{O}(L^2), \tag{4.7}$$

while for large L, f_{traction} approaches zero exponentially fast.

Thus, for small fiber length (providing it is longer than the diffusion length), the traction force exerted on the substrate increases linearly with length and in fact is the same as that in the large diffusion limit. This is not surprising: at small CF lengths, the friction relative to the cortex, which is distributed over the length, is negligible. When this friction is negligible, double integration of the force balance equation and taking into account the FA boundary conditions and that $\int_{-1/2}^{1/2} m(x)\, dx = 1$ gives the useful analytical result

$$f_{\text{traction}} = \frac{\beta}{2}, \tag{4.8}$$

which is equivalent to the dimensional expression $F_{\text{traction}} = \frac{k\zeta}{2\mu} \int_{-L/2}^{L/2} m(x)\, dx$.

Thus, in this limit, it does not matter whether myosin is distributed uniformly or aggregated into a cluster, or however else; all that matters is the total amount of myosin in the fiber.

For long fibers, the force exerted drops to zero exponentially. The reason is simple: the combination of cortex drag distributed along the length and gel viscosity causes decay of the myosin pull on the scale of L_{drag}. Therefore, the myosin cluster in the center is able to transduce only an exponentially small fraction of its stress to the FAs.

This implies that there is some intermediate length at which the fiber exerts maximal force. We could try to find this length by differentiating f_{traction} in (4.6) with respect to L, but this yields a complicated transcendental equation without a closed

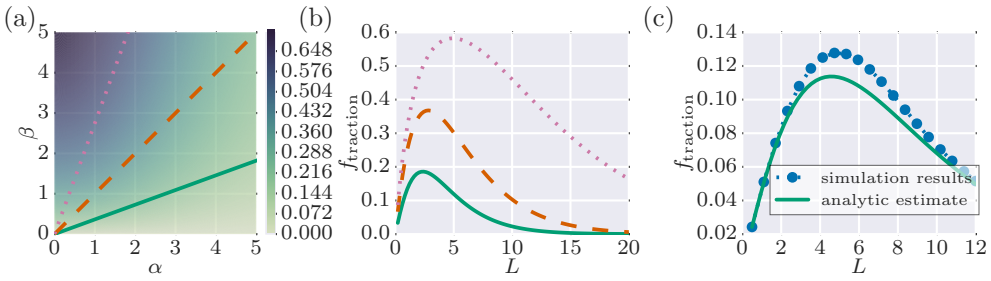

FIG. 4.1. *Force scaling for myosin clustered in a central peak.* (a) *Color plot of* $f_{traction}$ *from* (4.6) *with* $m_0 = 1$ *as a function of* α *and* β. *Since* α *and* β *scale linearly with* L, $f_{traction}$ *scales with length along a line from the origin in the* α-β *plane. Examples of such lines are shown.* (b) *Force scaling behavior for each of the lines shown in* (a). *In each case,* $f_{traction}$ *increases with* L *until it reaches a maximal value, after which it decays back to zero. Plots are in nondimensional units with the following scalings. Green, solid:* $\alpha = 0.9L$, $\beta = 0.3L$. *Orange, dashed:* $\alpha = 0.7L$, $\beta = 0.7L$. *Pink, dotted:* $\alpha = 0.3L$, $\beta = 0.9L$. (c) *Comparison of simulation results to the analytic scaling result obtained in section* 4 *for a stationary* δ*-function myosin distribution. Simulations were computed with* $\alpha = \frac{L}{2}$, $\beta = \frac{L}{10}$, *and* $\gamma = \frac{1}{L^2}$. *Color is available online only.*

form solution. Instead, we can gain insight into the qualitative behavior of f_{traction} at intermediate lengths by plotting it in the α-β plane, as shown in Figure 4.1a. Remember that $\alpha = \sqrt{\frac{\xi}{\mu}}L = \frac{L}{L_{\text{drag}}}$ and $\beta = \frac{\zeta}{\mu}L = \frac{L}{L_{\text{friction}}}$, and so both parameters are linear in L. Thus, as L varies, values of f_{traction} will fall along a line through the origin in the α-β plane. Such lines are shown in Figure 4.1a, and the resulting plots of L vs. f_{traction} for each line are shown in Figure 4.1b. We see indeed that for each line, f_{traction} increases with length up to a maximal value and then smoothly decays back to zero.

5. Numerical results. The δ-function ansatz is plausible, but we would like to see how force scales and how myosin and velocity distributions behave without making that approximation. To this end, we numerically solved the full model of (2.7)–(2.10) by using the numerical method described in section SM2 of the supplementary materials.

Figure 4.1c shows a typical force scaling result in the regime where $\alpha > \beta$. To produce this figure, we varied L for fixed values of the other length scales. For each value of L, we ran the numerical simulation to apparent steady state and then computed f_{traction}. As we can see from the figure, f_{traction} increases with L up to a maximal value and then decreases. This is consistent with our analysis based on the ansatz for the small diffusion limit. Indeed, it makes sense that our numerical result matches the force scaling in the small-diffusion limit: since $\gamma \propto L^{-2}$, as L increases, the fiber will inevitably end up in the parameter regime where $\alpha \gg \gamma$ and $\beta \gg \gamma$.

Unexpectedly, the force scaling results are quite different in the regime where $\alpha < \beta$. Figure 5.1 shows the typical behavior in this regime. As in the $\alpha > \beta$ regime, f_{traction} increases before beginning to plateau; however, f_{traction}'s rate of increase recovers, and it scales linearly with length even at high fiber lengths. This scaling behavior is not consistent with our ansatz analysis. As we show below, the reason is that the myosin peak in this regime aggregates to one of the CF ends and not to its center.

To understand the anomalous force scaling in Figure 5.1, we look in detail at the spatial distribution of myosin along our simulated SFs. Figures 5.2 and 5.3 show

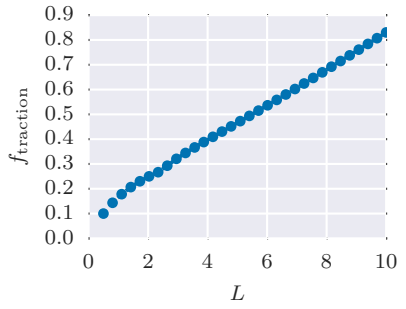

FIG. 5.1. *Force scaling in the regime where $\alpha < \beta$, which means that $L_{drag} < L_{friction}$ (actin cortex drag is less than FA friction). In this regime, force starts out increasing linearly with L, begins to plateau, and then recovers linear scaling. Simulations were computed with $\alpha = \frac{L}{10}$, $\beta = \frac{L}{2}$, and $\gamma = \frac{1}{L^2}$.*

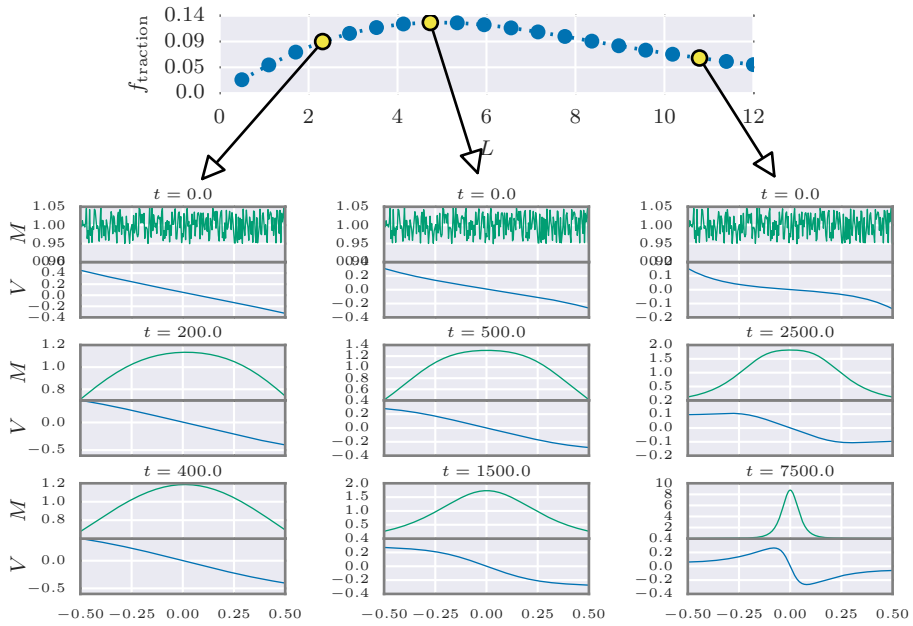

FIG. 5.2. *Force scaling and time-evolution of myosin distribution for $\alpha > \beta$. Top plot: Computational results showing force produced at steady-state as fiber length varies. Plots are in nondimensional units, with nondimensional parameters given by the scaling laws $\alpha = \frac{L}{2}$, $\beta = \frac{L}{10}$, and $\gamma = \frac{1}{L^2}$. Columns: Time-evolution of myosin distribution (green) and actin velocity (blue) from a perturbed initial condition for three specific fiber lengths. Color is available online only.*

the evolution of myosin from an initially perturbed constant distribution for several different values of L. Figure 5.2 shows this evolution for the case $\alpha > \beta$, while Figure 5.3 shows it for the case $\alpha < \beta$. We see that when $\alpha > \beta$, myosin clusters into a central peak. When $\alpha < \beta$, however, the behavior is more complicated. Myosin still forms a central peak; however, the peak then migrates from the center to one of the fiber edges.

Our numerical simulations therefore suggest the possibility of a symmetry-breaking

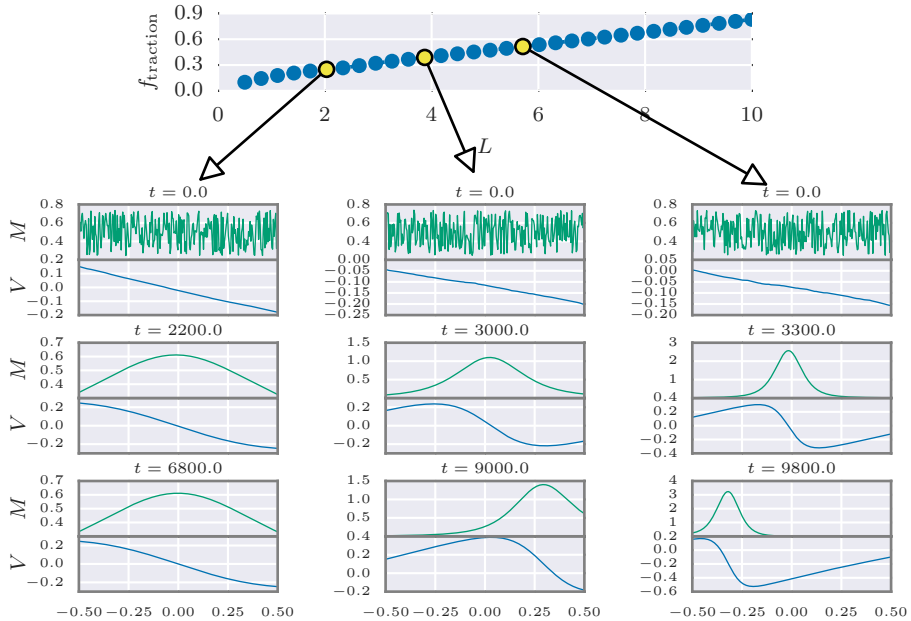

FIG. 5.3. *Force scaling and time-evolution of myosin distribution for $\alpha < \beta$. Top plot: Computational results showing force produced at steady-state as fiber length varies. Plots are in nondimensional units, with nondimensional parameters given by the scaling laws $\alpha = \frac{L}{10}$, $\beta = \frac{L}{2}$, and $\gamma = \frac{1}{L^2}$. Columns: Time-evolution of myosin distribution (green) and actin velocity (blue) from a perturbed initial condition for three specific fiber lengths. Color is available online only.*

bifurcation when $\alpha < \beta$. In the next section, we analyze this behavior in much greater detail to understand when and how the symmetry break occurs. For now, however, its appearance in our numerical results helps us understand why force scales linearly at high L when $\alpha < \beta$.

Recall from section 3 that f_{traction} was defined by

$$f_{\text{traction}} = \beta_l v\left(-\tfrac{1}{2}, t\right) + \max\left(f_{\text{drag}}, 0\right) = -\beta_r v\left(\tfrac{1}{2}, t\right) + \min\left(f_{\text{drag}}, 0\right),$$

where

$$f_{\text{drag}} = \alpha^2 \int_{-\frac{1}{2}}^{\frac{1}{2}} v(x,t)\, dx.$$

This definition resulted from our modeling choices in section 2 for both the drag-mediated fiber-cortex interaction and the transmission of force from cortex to FAs. Because the cortex is far stiffer than the fiber, we chose to model the cortex as an infinitely stiff structure. This meant that we could sum the contribution to the drag force on the cortex over the entire fiber to give the net drag force f_{drag}. To apply this net drag force to the substrate, we noted that typical FAs feel a pulling force from actin within the cell, so we chose to apply the entire quantity f_{drag} to whichever of the left or right FAs would feel that force as a pull.

Now we know, however, that this peak is capable of migrating to the fiber edge. The rightmost column of Figure 5.3 shows the actin velocity profile for a myosin peak located near the left fiber edge. Along most of the fiber, actin flows to the left. This means that f_{drag} will be a large pulling force applied to the right edge of

the fiber. Because this force is transmitted by the infinitely stiff cortex, there is no length-dependent dissipation of this force. Rather, the magnitude of the force grows with the total quantity of myosin in the cell, which leads to the linear force scaling observed in Figure 5.1.

The above analysis suggests that the linear force scaling for high lengths when $\alpha < \beta$ is a result of our simple representation of the cortex as a stiff solid object. Clearly, this modeling choice does not fully capture the mechanical nature of the cortex. We would expect that for long enough fibers, deformations of the cortex—while far smaller than deformations of the SF—would be important. For short enough fibers, however, the qualitative scaling behavior in Figure 5.1 is plausible: myosin clustering in the fiber center leads to a peak in force production, but once symmetry is broken, cortical stiffness allows force to start growing again. We expect, then, that for very large cells our model would need to be further developed to more fully account for cortical mechanics. In the meantime, however, it is clear that understanding the symmetry break shown in Figure 5.3 is vitally important.

6. Symmetry breaking in the small diffusion limit. Our numerical simulations suggest the possibility of a symmetry break, in which an initially small perturbation of a uniform myosin distribution leads to a myosin peak at one side of the fiber or the other. Furthermore, the numerical evidence hints that this peak goes to the center if $\alpha > \beta$, but if $\alpha < \beta$, there is a symmetry-breaking bifurcation and the peak aggregates to the edge. Such a bifurcation, however, may not exist. An alternative possibility is that symmetry always breaks, but that for large α our simulations lack the resolution to observe the myosin peak's slow migration away from the center. This would be true, for instance, if the peak's traveling speed were exponentially slow (see, e.g., [19, 23]). In this section, we show that in the limit $\gamma \to 0$, a symmetry-breaking bifurcation exists. Moreover, from that analysis we will derive simple expressions for the myosin distribution in both the symmetric and the asymmetric parameter regimes. Finally, we will provide a physical interpretation of these results with important implications for cell polarization.

In this section, we use a matched asymptotic expansion for $\gamma \ll 1$ to analyze the myosin distribution in the full model. This involves solving the model equations to find an outer solution that is valid for most of the CF, and matching that to an inner solution obtained by a change of length scale, which is valid for a small neighborhood around the center of the myosin peak.

One might be tempted to derive a matched asymptotic expansion of the variables m and v directly from the system of equations. However, both our intuition from section 4 and our numerical results from section 5 suggest that as γ approaches zero, $m(x,t)$ approaches a Dirac δ function. Thus, we cannot expect to match the leading-order term in m, which blows up, with the leading-order term in v, which remains $\mathcal{O}(1)$.

To overcome this difficulty, we rescale m. Let

$$\hat{m}(x,t) = \gamma m(x,t). \tag{6.1}$$

We will see that $\hat{m}$ remains bounded as $\gamma \to 0$, and this rescaling allows us to perform a useful matched asymptotic expansion.

In terms of $\hat{m}$, our system of equations is

$$\frac{\partial}{\partial x}\left(\gamma \frac{\partial v}{\partial x} + \hat{m}\right) = \alpha^2 \gamma v, \quad -\tfrac{1}{2} < x < \tfrac{1}{2}, \tag{6.2}$$

$$\gamma\frac{\partial v}{\partial x}+\hat{m}=\beta_l\gamma v\Big|_{x=-\frac{1}{2}},\quad \gamma\frac{\partial v}{\partial x}+\hat{m}=-\beta_r\gamma v\Big|_{x=\frac{1}{2}}, \tag{6.3}$$

$$\frac{\partial \hat{m}}{\partial t}+\frac{\partial}{\partial x}\Big(v\hat{m}\Big)=\gamma\frac{\partial^2\hat{m}}{\partial x^2},\quad -\tfrac{1}{2}<x<\tfrac{1}{2}, \tag{6.4}$$

$$v\hat{m}=\gamma\frac{\partial \hat{m}}{\partial x}\Big|_{x=\pm\frac{1}{2}}. \tag{6.5}$$

We expand both v and $\hat{m}$ in powers of γ, letting

$$v(x,t)=v_0(x,t)+\gamma v_1(x,t)+\mathcal{O}(\gamma^2), \tag{6.6}$$

$$\hat{m}(x,t)=\hat{m}_0(x,t)+\gamma\hat{m}_1(x,t)+\mathcal{O}(\gamma^2), \tag{6.7}$$

where $v_0, v_1, \ldots$ and $\hat{m}_0, \hat{m}_1, \ldots$ are independent of γ.

Substituting our expansions into the model equations and matching like powers of γ, we get the zeroth-order outer equations

$$\frac{\partial \hat{m}_0}{\partial x}=0,\quad -\tfrac{1}{2}<x<\tfrac{1}{2}, \tag{6.8}$$

$$\hat{m}_0\Big(\pm\tfrac{1}{2},t\Big)=0, \tag{6.9}$$

$$\frac{\partial \hat{m}_0}{\partial t}+\frac{\partial}{\partial x}\Big(v_0\hat{m}_0\Big)=0,\quad -\tfrac{1}{2}<x<\tfrac{1}{2}, \tag{6.10}$$

$$v_0\Big(\pm\tfrac{1}{2},t\Big)\hat{m}_0\Big(\pm\tfrac{1}{2},t\Big)=0. \tag{6.11}$$

From (6.8) and (6.9) it trivially follows that $\hat{m}_0(x,t)=0$ for all x and t. This makes physical sense, since $\frac{1}{\gamma}\hat{m}(x,t)=m(x,t)$. If $\hat{m}_0$ were nonzero, then as $\gamma\to 0$ the density m of myosin would approach infinity.

Using $\hat{m}_0=0$, the first-order outer equations are

$$\frac{\partial}{\partial x}\left(\frac{\partial v_0}{\partial x}+\hat{m}_1\right)=\alpha^2 v_0,\quad -\tfrac{1}{2}<x<\tfrac{1}{2}, \tag{6.12}$$

$$\frac{\partial v_0}{\partial x}+\hat{m}_1=\beta_l v_0\Big|_{x=-\frac{1}{2}}, \tag{6.13}$$

$$\frac{\partial v_0}{\partial x}+\hat{m}_1=-\beta_r v_0\Big|_{x=\frac{1}{2}}, \tag{6.14}$$

$$\frac{\partial \hat{m}_1}{\partial t}+\frac{\partial}{\partial x}\Big(v_0\hat{m}_1\Big)=0,\quad -\tfrac{1}{2}<x<\tfrac{1}{2}, \tag{6.15}$$

$$v_0\Big(\pm\tfrac{1}{2},t\Big)\hat{m}_1\Big(\pm\tfrac{1}{2},t\Big)=0. \tag{6.16}$$

This is a nonlinear system with many possible solutions. However, as we mentioned a moment ago, $\frac{1}{\gamma}\hat{m}(x,t)=m(x,t)$. This means that $m(x,t)=\hat{m}_1(x,t)+\mathcal{O}(\gamma)$. Since we expect that m will approach a δ function as $\gamma\to 0$, this suggests that $\hat{m}_1(x,t)=0$ is the physically correct solution; otherwise, the myosin density would remain nonzero over the whole fiber regardless of how small γ became.

Thus, the first-order outer equations simplify to the linear boundary value problem

$$\frac{\partial^2 v_0}{\partial x^2}=\alpha^2 v_0,\quad -\tfrac{1}{2}<x<\tfrac{1}{2}, \tag{6.17}$$

$$\frac{\partial v_0}{\partial x}=\beta_l v_0\Big|_{x=-\frac{1}{2}},\quad \frac{\partial v_0}{\partial x}=-\beta_r v_0\Big|_{x=\frac{1}{2}}. \tag{6.18}$$

The general solution to (6.17) is

$$v_0(x,t) = c_0(t)\sinh \alpha x + c_1(t)\cosh \alpha x \tag{6.19}$$

for the yet-to-be-determined real coefficients $c_0(t)$ and $c_1(t)$.

It would not be fruitful to compute the coefficients $c_0(t)$ and $c_1(t)$ from the boundary conditions in (6.18). That would correspond to the physically uninteresting solution where m is identically zero throughout the whole fiber. If there is myosin present in the fiber, then we expect it to cluster in some small region. In that region, the diffusive term in (6.4) will be nonnegligible, and we need to perform a change of variables to find the inner solution valid in that region. Intuitively, this region corresponds to the location of the δ function peak we posited in section 4.

Let $x_0(t)$ be the (unknown) location of this myosin peak, and define the inner variables $V(X,t)$ and $\hat{M}(X,t)$ by

$$V\left(\frac{x - x_0(t)}{\gamma}, t\right) = v(x,t) \tag{6.20}$$

and

$$\hat{M}\left(\frac{x - x_0(t)}{\gamma}, t\right) = \hat{m}(x,t). \tag{6.21}$$

In terms of X, V, and $\hat{M}$, our system of equations becomes

$$\frac{\partial^2 V}{\partial X^2} + \frac{\partial \hat{M}}{\partial X} = \alpha^2\gamma^2 V, \tag{6.22}$$

$$\gamma\frac{\partial \hat{M}}{\partial t} - x_0'(t)\frac{\partial \hat{M}}{\partial X} + \frac{\partial}{\partial X}(\hat{M}V) = \frac{\partial^2 \hat{M}}{\partial X^2}. \tag{6.23}$$

We expand V and $\hat{M}$ in powers of γ:

$$V(X,t) = V_0(X,t) + \gamma V_1(X,t) + \mathcal{O}(\gamma^2), \tag{6.24}$$

$$\hat{M}(X,t) = \hat{M}_0(X,t) + \gamma\hat{M}_1(X,t) + \mathcal{O}(\gamma^2). \tag{6.25}$$

This gives the zeroth-order inner equations

$$\frac{\partial^2 V_0}{\partial X^2} + \frac{\partial \hat{M}_0}{\partial X} = 0, \tag{6.26}$$

$$-x_0'(t)\frac{\partial \hat{M}_0}{\partial X} + \frac{\partial}{\partial X}(\hat{M}_0 V_0) = \frac{\partial^2 \hat{M}_0}{\partial X^2}. \tag{6.27}$$

We can solve (6.26) for $\hat{M}_0$ by integration, getting

$$\hat{M}_0(X,t) = -\frac{\partial V_0}{\partial X} + C_0(t). \tag{6.28}$$

We can substitute this expression into (6.27) and integrate by X, giving a single differential equation for V_0:

$$\left(C_0(t) - \frac{\partial V_0}{\partial X}\right)\left(V_0 - x_0'(t)\right) = -\frac{\partial^2 V_0}{\partial X^2} + C_1(t). \tag{6.29}$$

In general, solutions to (6.26) and (6.27) may exist for many values of the constants of integration $C_0(t)$ and $C_1(t)$. For our purposes, all that any particular solution needs to do to be useful is provide enough degrees of freedom to match with the outer solutions. As we will see, such a solution comes from simply setting $C_0(t) = C_1(t) = 0$. In this case, the differential equation for V_0 simplifies to

$$-\frac{\partial V_0}{\partial X}\big(V_0 - x_0'(t)\big) = -\frac{\partial^2 V_0}{\partial X^2}, \tag{6.30}$$

which has the solution

$$V_0(X,t) = x_0'(t) - \sqrt{x_0'(t)^2 - 2C(t)}\tanh\left(\sqrt{x_0'(t)^2 - 2C(t)}\frac{X}{2}\right). \tag{6.31}$$

6.1. Matching. Our solution in the transition layer located at $x = x_0(t)$ is

$$V_0(X,t) = x_0'(t) - \sqrt{x_0'(t)^2 - 2C(t)}\tanh\left(\sqrt{x_0'(t)^2 - 2C(t)}\frac{X}{2}\right), \tag{6.32}$$

$$M_0(X,t) = -\frac{\partial V_0}{\partial X}. \tag{6.33}$$

On either side of this transition layer, the outer solution is a linear combination of $\sinh \alpha x$ and $\cosh \alpha x$, which we can write as

$$v_0(x,t) = c_0(t)\sinh \alpha x + c_1(t)\cosh \alpha x, \quad -\tfrac{1}{2} < x < x_0(t), \tag{6.34}$$

$$v_0(x,t) = c_3(t)\sinh \alpha x + c_4(t)\cosh \alpha x, \quad x_0(t) < x < \tfrac{1}{2}. \tag{6.35}$$

These equations have six unknowns: the five constants of integration $c_0(t)$, $c_1(t)$, $c_2(t)$, $c_3(t)$, $c_4(t)$, and $C(t)$ and the term $x_0'(t)$.

To solve for our six unknowns we need six equations. Some of these equations are immediately available: the boundary conditions on v_0 and the continuity of the inner and outer solutions. These give the equations

$$\frac{\partial v_0}{\partial x} = \beta_l v_0\Big|_{x=-\frac{1}{2}}, \quad \frac{\partial v_0}{\partial x} = -\beta_r v_0\Big|_{x=\frac{1}{2}} \tag{6.18}$$

and

$$\lim_{x\to x_0(t)^{\pm}} = \lim_{X\to\pm\infty} V_0(X,t). \tag{6.36}$$

Evaluating these limits allows us to rewrite the continuity condition as

$$c_0(t)\sinh \alpha x_0(t) + c_1(t)\cosh \alpha x_0(t) = x_0'(t) + \sqrt{x_0'(t)^2 - 2C(t)}, \tag{6.37}$$

$$c_3(t)\sinh \alpha x_0(t) + c_4(t)\cosh \alpha x_0(t) = x_0'(t) - \sqrt{x_0'(t)^2 + 2C(t)}. \tag{6.38}$$

Together, (6.18), (6.37), and (6.38) give us four equations for our six unknowns.

A fifth equation comes from treating the total amount of myosin in the fiber as known. Recall that our outer solution for myosin was $\hat{m}_0 = \hat{m}_1 = 0$. This means that to leading order, all myosin in the SF is contained in the transition layer around $x_0(t)$. Since we nondimensionalized myosin in terms of its average density,

$$1 = \int_{-\frac{1}{2}}^{\frac{1}{2}} m(x,t)\, dx. \tag{6.39}$$

Then

$$1 = \int_{-\frac{1}{2}}^{\frac{1}{2}} \frac{\hat{m}(x,t)}{\gamma}\, dx. \tag{6.40}$$

Since $\hat{m}_0 = \hat{m}_1 = 0$, this means that

$$\begin{aligned} 1 &= \int_{-\frac{1}{2}}^{\frac{1}{2}} \frac{\hat{M}\left(\frac{x-x_0(t)}{\gamma}, t\right)}{\gamma}\, dx \\ &= \int_{-\infty}^{\infty} \hat{M}(X,t)\, dX \end{aligned} \tag{6.41}$$

for $\gamma \ll 1$.

A sixth and final equation comes from stress balance across the transition layer. There are two ways to derive this equation: by physical argument and by higher-order matching of the inner and outer solutions using an intermediate variable. We prefer the first way.

The physical argument is quite simple. The only way for stress to leave the fiber is through drag against the cortex. This drag is governed by a coefficient of the form force per velocity per length. Since the transition layer is very small, and since velocity is continuous and $\mathcal{O}(1)$ in the layer, only a negligible amount of force should be transmitted from the fiber to the cortex over the length of the transition layer. This means that the stress computed from the outer solutions on either side of the layer should be equal:

$$\left.\frac{\partial v_0}{\partial x}\right|_{x=x_0(t)^-} = \left.\frac{\partial v_0}{\partial x}\right|_{x=x_0(t)^+} \tag{6.42}$$

or

$$c_0\alpha\cosh\alpha x_0 + c_1\alpha\sinh\alpha x_0 = c_2\alpha\cosh\alpha x_0 + c_3\alpha\sinh\alpha x_0, \tag{6.43}$$

giving us the final equation we need to solve for our unknowns.

Equations (6.18), (6.37), (6.38), (6.41), and (6.43) together give us six algebraic equations for the unknowns $c_0(t)$, $c_1(t)$, $c_2(t)$, $c_3(t)$, $c_4(t)$, $C(t)$, and $x_0'(t)$. It is a simple, albeit lengthy, exercise to solve for all six.

We do not write out expressions for all six unknowns. The five constants of integration are mainly important for computing the actin velocity profile $v(x,t)$. We are only interested in the myosin peak, whose dynamics are governed by $x_0'(t)$. Solving for $x_0'(t)$, we get the ODE

$$x_0'(t) = \frac{\alpha\cosh\Big(2\alpha x_0(t)\Big)(\beta_r - \beta_l) + \sinh\Big(2\alpha x_0(t)\Big)(\beta_r\beta_l - \alpha^2)}{2\alpha\cosh(\alpha)(\beta_r + \beta_l) + 2\sinh(\alpha)(\alpha^2 + \beta_r\beta_l)}. \tag{6.44}$$

Setting $x_0'(t) = 0$, we can solve for the steady-state value $\overline{x_0}$:

$$\overline{x_0} = \frac{1}{2\alpha}\log\sqrt{\frac{(\alpha-\beta_l)(\alpha+\beta_r)}{(\alpha+\beta_l)(\alpha-\beta_r)}}. \tag{6.45}$$

From (6.45), it is apparent that $\overline{x_0}$ is only real-valued if either

$$\beta_l < \alpha \quad \text{and} \quad \beta_r < \alpha \tag{6.46}$$

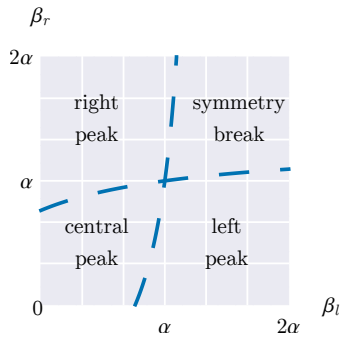

FIG. 6.1. *Physical stability for $\alpha = 1$ in the β_l-β_r plane. In the bottom left region, the fixed point $\overline{x_0}$ exists, is stable, and is in the fiber interior between $-\frac{1}{2}$ and $\frac{1}{2}$. In the top right region, it exists and is in the fiber interior but is unstable. In the bottom right region, either no steady-state exists or $\overline{x_0} < -\frac{1}{2}$; in either case, the myosin peak migrates all the way to the left edge of the SF. Similarly, in the top left region, the myosin peak migrates all the way to the right edge of the SF.*

or

$$\alpha < \beta_l \quad \text{and} \quad \alpha < \beta_r. \tag{6.47}$$

In fact, from (6.44), it is straightforward to show that if neither of these conditions holds, then $x_0'(t)$ is either always positive (when $\beta_l < \alpha < \beta_r$) or always negative (when $\beta_r < \alpha < \beta_l$).

Moreover, even when $\overline{x_0}$ exists and is real, from (6.45) we can find conditions for which it is outside the physical domain $-\frac{1}{2} < x < \frac{1}{2}$. This means that even though a steady-state exists, $x_0'(t)$ is still either always positive or always negative for all physically relevant values of $x_0(t)$. Mathematically, this corresponds to the case where the stable steady-state of the full PDE system does not exhibit a transition layer in the interior of the domain but instead has a boundary layer at either $x = -\frac{1}{2}$ or $x = \frac{1}{2}$.

Figure 6.1 shows the physical stability of $\overline{x_0}$ in the β_l-β_r plane for a fixed value of α. Here parameter space is divided into four sections: the upper left and the lower right regions correspond to the cases where either $\overline{x_0}$ is complex or $|\overline{x_0}| > \frac{1}{2}$. In the upper left, $x_0'(t) > 0$ for all $x_0(t)$ between $-\frac{1}{2}$ and $\frac{1}{2}$, and in the lower right $x_0'(t) < 0$.

In the lower right region where $\beta_l < \alpha$ and $\beta_r < \alpha$, $\overline{x_0}$ exists, is between $-\frac{1}{2}$ and $\frac{1}{2}$, and is a stable steady-state. This means that once myosin has formed a sharp transition layer, that peak will migrate to $\overline{x_0}$, which is in the interior of the fiber. In particular, note that $\overline{x_0} = 0$ when $\beta_l = \beta_r$, so that the stable steady-state is in the center of the fiber.

In the upper left region where $\alpha < \beta_l$ and $\alpha < \beta_r$, $\overline{x_0}$ also exists and is in the physical domain but is an unstable steady-state. In this region of parameter space, the initial location of the myosin peak determines whether it will move to the left or to the right of the fiber.

We observe the same stability properties for different values of α (see Figure SM3 in the supplementary materials). In each case, the steady-state behavior is qualitatively similar, but as α decreases, β_l and β_r must be closer in value to one another in order for a physically meaningful steady-state to exist.

6.2. Physical interpretation. The steady-state analysis that follows from (6.44) and (6.45) shows that the symmetry-breaking bifurcation that we observed

numerically in section 5 is a real phenomenon that occurs when α is smaller than both β_l and β_r. Moreover, the specific conditions under which the symmetry break occurs give us insight into the physical mechanism driving the motion of the myosin peak.

The peak's motion is governed by a combination of local and distributed effects: adhesion-mediated local forces at the left and right fiber edges and drag-mediated distributed forces spread over the entire domain. The critical difference between these two effects is that if myosin is off-center, the adhesive forces act to exaggerate that asymmetry by pulling myosin even further to one side, while the drag forces promote recentering of the myosin peak.

We can see the tendency of adhesion-mediated forces to promote asymmetry by recalling the length-scale discussion from section 3. There we found that we could express the adhesion friction coefficients by

$$\beta_{l,r} = \frac{L}{L_{\text{friction}\,l,r}}, \tag{6.48}$$

where L_{friction} is a measure of the decay length scale of adhesive forces generated at the fiber edge. Thus, the closer the myosin peak is to an edge, the less decay of that adhesive force there will be and the more strongly myosin will be pulled toward that edge.

The distributed cortex-drag-mediated forces have the opposite effect. The magnitude of this drag force scales like length times velocity. This means that when myosin exerts a contractile stress at a point along the fiber, the drag force produced on either side of the peak will be roughly proportional to the fraction of the fiber length that is on that side of the peak. This means that if the peak is close to the center of the cell, the drag force it feels from the left and right sides of the fiber will be equal and opposite. If, on the other hand, the peak is very close to one side of the fiber, the drag force it feels will be almost entirely in the direction of the far-off side.

Thus, drag forces promote myosin centering, while adhesive forces promote symmetry breaking. We see in the stability diagrams of Figure SM3 in the supplementary materials and Figure 6.1 that, depending on the magnitude of the cortex drag and adhesion friction coefficients, one or the other of these two effects dominates. When α is small compared to β_l and β_r, the symmetry-breaking effect wins, while when α is large, the centering effect wins. When $\overline{x_0}$ does not exist, α is strong enough that centering effects dominate one of the two adhesions but not the other.

7. Discussion. We found that three length scales govern the myosin and velocity distributions and force generation in the model CF. When the CF length is less than the diffusion length, myosin is distributed almost uniformly across the CF; the traction force first increases linearly with CF length and then starts to plateau to the value determined by the adhesion strengths. When the CF length becomes greater than the diffusion length, positive feedback between the actin gel flow and myosin-powered force drives myosin into an aggregate. The position of this peak in the myosin distribution is determined by the relation between the adhesion and cortex drag lengths. If the former is greater (adhesion to the actin cortex is stronger than the FAs), then the peak is located at the center of the CF, because the length-dependent centering pull of the connections between the CF and the cortex is stronger than the effective pull of the FAs. In this case, the traction force, after reaching a maximum at an intermediate CF length, decreases in longer CFs, because the myosin effect is wasted on the cortex drag.

On the other hand, if the adhesion length is smaller than the drag length (adhesion to the actin cortex is weaker than the FAs), then the peak shifts to one of the edges, because the pull to one of the FAs is stronger than the centering effect of the cortex. In this case, the traction force keeps growing with increasing CF length, because the amount of myosin accumulating at the CF edge increases linearly with the CF length and is able to generate greater stress. Our model also makes specific and testable predictions about the force dependence on the CF length.

The model we considered in this paper is closest to the study [6]. One minor difference between that study and our model is that we consider contractile stress to be linearly proportional to the myosin density, m, while there the stress is proportional to $\frac{m}{m+1}$. This difference is not very consequential; more important is that instead of a periodic boundary condition for the force balance equation in [6], which is very appropriate to contractile rings, we use a nontrivial balance between viscous, contractile, and adhesive force at the CF ends. This allows us to investigate traction forces, which were not studied in [6], and allows us to find nontrivial scaling of these forces with the fiber's length. Moreover, though the phenomenon of myosin peak formation was predicted in [6], our model addresses the previously unexamined question of the location of these peaks and predicts the phenomenon of a symmetry break.

The model's applicability to SFs in nonmuscle cells is not a straightforward issue. SFs are often observed to have a periodic sarcomeric structure and are thought of as very steady and nondynamic minimuscles [16, 34]. However, recent studies and reviews show that what was called "the stress fiber" previously is actually a growing inventory of diverse one-dimensional contractile networks with very complex dynamic structure [30, 49]. A periodic myosin pattern was reported in some, but not all, SFs [20]. Specifically, both uniform myosin density along fibers in vivo [27, 50] and in vitro [47], as well as aperiodic bands and small myosin aggregates along the fibers, have been reported [40, 43]. Similarly, both uniform and nonuniform but continuous and aperiodic myosin densities were reported in contractile rings [55]. Moreover, experimental measurements have revealed that SFs (at least, a number of types of stress fibers) are not steady: centripetal actin flow near the fibers' ends was observed [48], and myosin turnover on the scale of ~ 100 / sec has been observed [20, 31, 45].

We emphasize, again, that we do not address SF dynamics on microscopic, micron and submicron, scales that involve subtle spatial-temporal patterns of myosin and crosslinker densities and actin polarity (see, for example, [17, 43]). Nor does our model address distinctions between different types of SFs. Rather, we consider a more general and macroscopic model of a contractile actin-myosin gel, assuming that elementary contractile units are organized at the micron and submicron scales and that the continuous density approximation for the gel made of these units is justified.

What parameters are characteristic of SFs? The fibers' size, L, varies widely, from a few microns to tens of microns. The order of magnitude of the myosin turnover rate is $k_{\text{off}} \sim 0.01\,\text{s}^{-1}$ [20, 31, 45]. The speed of the inward flow near the fiber's ends is on the order of $v \sim 0.01\,\mu\text{m}\,\text{s}^{-1}$ [1] and likely much slower away from the ends [48]. Thus, assuming that (2.3) describes myosin transport in SFs, $\frac{v}{Lk_{\text{off}}} \ll 1$, and so the prediction would be that myosin is distributed almost uniformly along the fiber length, in agreement with the observations described above. Isolated SFs contract telescopically at the rate $\sim 0.1\,\text{s}^{-1}$ [22], which is also true for in vitro actin-myosin bundles [47] (this rate is estimated as the speed of contraction, which is proportional to the fiber length, divided by the length). These isolated fibers have no friction relative to the cortex, and FAs at their ends are removed, and so, according to our theory, the force balance in these fibers is $\mu\frac{dv}{dx} \sim km$. The myosin generated force,

km, is on the order of 100 pN [1, 42], so the effective viscosity can be estimated as $\mu \sim km/\frac{dv}{dx} \sim 10^3\,\mathrm{pN} \times \mathrm{s}$. The FA friction coefficient can be estimated as the generated force divided by the flow rate, on the order of $0.01\,\mu\mathrm{m\,s}^{-1}$, so $\zeta \sim 10^4\,\mathrm{pN} \times \mathrm{s}/\mu\mathrm{m}$. Thus, the ratio $\mu/\zeta \sim 0.1\,\mu\mathrm{m}$ is much smaller than the fiber's length, and so the model prediction would be that the SF generates a maximal force that depends very weakly on the fiber's length. In addition, though the cortex drag coefficient was never measured, indirect observations suggest that it is very significant [5, 44]. This drag would further dampen the length dependence of the traction force.

There are many caveats to these estimates, the main of which is that there is a significant elasticity associated with SFs [11, 26]; besides, we used estimates from very different experimental systems and conditions. To truly test the model's predictions, a challenging experimental assay has to be put together, in which the strength of micropatterned adhesions has to be controlled, as well as friction between the fiber and the surrounding actin network. In addition, traction forces, myosin density, and the fiber's viscosity must be measured at varied distances from the adhesions. Perhaps the best way would be to start from experiments in vitro, by measuring traction forces in reconstituted CFs stretched between two adhesive spots printed on a flexible substrate [15].

Finally, there is the issue of FA dynamics at the fiber's ends. In the model, we assumed the FAs to be immobile, which is, in fact, often observed for SFs [7]. This is easily reconciled with the flow of the actomyosin gel at the ends of the fiber, as the actin mesh is constantly polymerizing and slipping centripetally from the edges inward [4, 48]. This phenomenon is likely dependent on formins that co-localize with adhesion molecules and keep actin polymerization going [4]. How the rate of the polymerization process is regulated to keep it equal to the rate of the actin centripetal flow is an open problem. However, there are also cases where the adhesion complexes are either slipping inward relative to the substrate or extending outward [48]. There is currently no clear understanding of the underlying complex molecular processes that would warrant a mathematical model of these cases [4]. Qualitatively, there are two simple limiting cases. Assuming that there is no actin polymerization at the fiber ends, the ends would be moving inward with a velocity predicted by the solution of the force balance equation of our model. In one limiting case, when the effective myosin diffusion or recycling is much faster than the myosin drift, the rate of change of the fiber's length will be much slower than the rates of myosin redistribution and of velocity and stress equilibration. In the zeroth approximation, in this limiting case all solutions for the constant fiber's length are valid; the only change would be that the length, $L(t)$, becomes a function of time, governed by equation $\frac{dL}{dt} = 2v\left(\frac{L}{2}\right)$, where $v\left(\frac{L}{2}\right)$ is given by the solution of the stationary problem. In another limiting case, with slow myosin diffusion and a peak at the center, the picture is exactly the same: the peak remains at the center, while the fiber's length decreases according to equation $\frac{dL}{dt} = 2v\left(\frac{L}{2}\right)$. Finally, when the peak is expected to be at the end of the fiber, it is qualitatively clear that the myosin aggregate will stay at this end, because this end moves inward faster than the other end.

This model could also be relevant to contractile rings in cytokinesis. These rings contract telescopically [9] and exhibit myosin turnover on a finite time scale [33, 41]. The myosin-generated tension in the rings has been measured. However, the adhesions and drag between the ring and the cell cortex would have to be much better characterized before quantitative estimates could be made [36].

Finally, the model is also applicable to lamellipodial/lamellar actomyosin net-

works, with the caveat that these networks are two-dimensional, rather than one-dimensional. In some cases, however, flat lamellipodial networks are such that their width, for example, is significantly greater than their length, as in the case of motile fish keratocyte cells [3, 39]. Interestingly, large myosin aggregates that were not observed in individual SFs were observed in these lamellipodial networks [3], which is explained by the fact that in these networks the myosin dissociation rate is so slow that myosin clusters travel across the cell before they detach from the network [39]. The condition for the symmetry break predicted by our model is the following: adhesion at the edges has to be stronger than the drag distributed along the network length. Thus, our analysis suggests a simple mechanism for cell symmetry maintenance and for cell polarization. To remain symmetric, a cell simply needs to ensure that adhesive drag along the cell length is stronger than the adhesions at the cell edges. This is likely the case in keratocytes, and indeed the mechanism of their polarization is based on a nonlinear dependence of the adhesion strength on the network flow [2]. Our model suggests that a cell can achieve—or prevent—polarization by another mechanism: regulating the relative strength of the adhesions along the cell length and at the cell edges. Other potential mechanisms were modeled in [2, 8, 24, 38]; future work will be needed to see what combination of the proposed mechanisms applies in which types of cells.

Our model has many limitations: we assumed a constant average myosin density, so that total myosin scales with CF length. Actual myosin scaling with length could be different. Simple linear constitutive relations between myosin strength and its density and between friction forces and velocities could be highly nonlinear. It is likely that the CF gel is viscoelastic, rather than simply viscous [11, 26]. Effective actin-myosin gel viscosity could, similarly, depend on actin density, in which case the model would need to be expanded by adding an equation for actin transport and turnover. The model does not address microscopic phenomena that give rise to the periodicity of myosin and crosslinking distributions on submicron scales [16, 34], nor does it address the subtle distinction between different types of SFs [49]. Last, but not least, we did not include mechanosensing phenomena in the model [11]. Nevertheless, the model clearly illustrates the wealth of behavior in even the simplest mechanical case. Comprehensive mathematical elucidation of this behavior is the necessary first step on the way to quantitative understanding of the full biological complexity of contractile actin-myosin networks.

REFERENCES

[1] Y. Aratyn-Schaus, P. W. Oakes, and M. L. Gardel, *Dynamic and structural signatures of lamellar actomyosin force generation*, Mol. Biol. Cell, 22 (2011), pp. 1330–1339, https://doi.org/10.1091/mbc.E10-11-0891.

[2] E. Barnhart, K.-C. Lee, G. M. Allen, J. A. Theriot, and A. Mogilner, *Balance between cell–substrate adhesion and myosin contraction determines the frequency of motility initiation in fish keratocytes*, Proc. Natl. Acad. Sci. USA, 112 (2015), pp. 5045–5050, https://doi.org/10.1073/pnas.1417257112.

[3] E. L. Barnhart, K. C. Lee, K. Keren, A. Mogilner, and J. A. Theriot, *An adhesion-dependent switch between mechanisms that determine motile cell shape*, PLoS Biol., 9 (2011), e1001059, https://doi.org/10.1371/journal.pbio.1001059.

[4] A. D. Bershadsky, C. Ballestrem, L. Carramusa, Y. Zilberman, B. Gilquin, S. Khochbin, A. Y. Alexandrova, A. B. Verkhovsky, T. Shemesh, and M. M. Kozlov, *Assembly and mechanosensory function of focal adhesions: Experiments and models*, Eur. J. Cell Biol., 85 (2006), pp. 165–173, https://doi.org/10.1016/j.ejcb.2005.11.001.

[5] A. Besser, J. Colombelli, E. H. K. Stelzer, and U. S. Schwarz, *Viscoelastic response of contractile filament bundles*, Phys. Rev. E (3), 83 (2011), 051902, https://doi.org/10.1103/

PhysRevE.83.051902.

[6] J. S. Bois, F. Jülicher, and S. W. Grill, *Pattern formation in active fluids*, Phys. Rev. Lett., 106 (2011), 028103, https://doi.org/10.1103/PhysRevLett.106.028103.

[7] K. Burridge and E. S. Wittchen, *The tension mounts: Stress fibers as force-generating mechanotransducers*, J. Cell Biol., 200 (2013), pp. 9–19, https://doi.org/10.1083/jcb.201210090.

[8] A. E. Carlsson, *Mechanisms of cell propulsion by active stresses*, New J. Phys., 13 (2011), 073009, https://doi.org/10.1088/1367-2630/13/7/073009.

[9] A. Carvalho, A. Desai, and K. Oegema, *Structural memory in the contractile ring makes the duration of cytokinesis independent of cell size*, Cell, 137 (2009), pp. 926–937, https://doi.org/10.1016/j.cell.2009.03.021.

[10] A. G. Clark, O. Wartlick, G. Salbreux, and E. K. Paluch, *Stresses at the cell surface during animal cell morphogenesis*, Curr. Biol., 24 (2014), pp. R484–R494, https://doi.org/10.1016/j.cub.2014.03.059.

[11] J. Colombelli, A. Besser, H. Kress, E. G. Reynaud, P. Girard, E. Caussinus, U. Haselmann, J. V. Small, U. S. Schwarz, and E. H. K. Stelzer, *Mechanosensing in actin stress fibers revealed by a close correlation between force and protein localization*, J. Cell Sci., 122 (2009), pp. 1928–1928, https://doi.org/10.1242/jcs.054577.

[12] G. Danuser, J. Allard, and A. Mogilner, *Mathematical modeling of eukaryotic cell migration: Insights beyond experiments*, Annu. Rev. Cell Dev. Biol., 29 (2013), pp. 501–528, https://doi.org/10.1146/annurev-cellbio-101512-122308.

[13] A. D. Doyle, M. L. Kutys, M. A. Conti, K. Matsumoto, R. S. Adelstein, and K. M. Yamada, *Micro-environmental control of cell migration - myosin IIA is required for efficient migration in fibrillar environments through control of cell adhesion dynamics*, J. Cell Sci., 125 (2012), pp. 2244–2256, https://doi.org/10.1242/jcs.098806.

[14] E. L. Elson and G. M. Genin, *The role of mechanics in actin stress fiber kinetics*, Exp. Cell Res., 319 (2013), pp. 2490–2500, https://doi.org/10.1016/j.yexcr.2013.06.017.

[15] H. Ennomani, G. Letort, C. Guérin, J. L. Martiel, W. Cao, F. Nédélec, E. M. De La Cruz, M. Théry, and L. Blanchoin, *Architecture and connectivity govern actin network contractility*, Curr. Biol., 26 (2016), pp. 616–626, https://doi.org/10.1016/j.cub.2015.12.069.

[16] B. M. Friedrich, A. Buxboim, D. E. Discher, and S. A. Safran, *Striated acto-myosin fibers can reorganize and register in response to elastic interactions with the matrix*, Biophys. J., 100 (2011), pp. 2706–2715, https://doi.org/10.1016/j.bpj.2011.04.050.

[17] B. M. Friedrich, E. Fischer-Friedrich, N. S. Gov, and S. A. Safran, *Sarcomeric pattern formation by actin cluster coalescence*, PLoS Comput. Biol., 8 (2012), e1002544, https://doi.org/10.1371/journal.pcbi.1002544.

[18] M. L. Gardel, I. C. Schneider, Y. Aratyn-Schaus, and C. M. Waterman, *Mechanical integration of actin and adhesion dynamics in cell migration*, Annu. Rev. Cell Dev. Biol., 26 (2010), pp. 315–333, https://doi.org/10.1146/annurev.cellbio.011209.122036.

[19] M. H. Holmes, *Introduction to Perturbation Methods*, Texts Appl. Math. 20, Springer, New York, 2013, https://doi.org/10.1007/978-1-4614-5477-9.

[20] P. Hotulainen and P. Lappalainen, *Stress fibers are generated by two distinct actin assembly mechanisms in motile cells*, J. Cell Biol., 173 (2006), pp. 383–394, https://doi.org/10.1083/jcb.200511093.

[21] P. Kanchanawong, G. Shtengel, A. M. Pasapera, E. B. Ramko, M. W. Davidson, H. F. Hess, and C. M. Waterman, *Nanoscale architecture of integrin-based cell adhesions*, Nature, 468 (2010), pp. 580–584, https://doi.org/10.1038/nature09621.

[22] K. Katoh, Y. Kano, M. Masuda, H. Onishi, and K. Fujiwara, *Isolation and contraction of the stress fiber*, Mol. Biol. Cell, 9 (1998), pp. 1919–1938, https://doi.org/10.1091/MBC.9.7.1919.

[23] J. P. Keener, *Principles of Applied Mathematics: Transformation and Approximation*, Perseus Books, Cambridge, MA, 2000.

[24] L. S. Kimpton, J. P. Whiteley, S. L. Waters, J. R. King, and J. M. Oliver, *Multiple travelling-wave solutions in a minimal model for cell motility*, Math. Med. Biol., 30 (2013), pp. 241–272, https://doi.org/10.1093/imammb/dqs023.

[25] S. Kumar, I. Z. Maxwell, A. Heisterkamp, T. R. Polte, T. P. Lele, M. Salanga, E. Mazur, and D. E. Ingber, *Viscoelastic retraction of single living stress fibers and its impact on cell shape, cytoskeletal organization, and extracellular matrix mechanics*, Biophys. J., 90 (2006), pp. 3762–3773, https://doi.org/10.1529/biophysj.105.071506.

[26] C. Labouesse, C. Gabella, J. J. Meister, B. Vianay, and A. B. Verkhovsky, *Microsurgery-aided in-situ force probing reveals extensibility and viscoelastic properties*

of individual stress fibers, Sci. Rep., 6 (2016), 23722, https://doi.org/10.1038/srep23722.

[27] C. Labouesse, A. B. Verkhovsky, J. J. Meister, C. Gabella, and B. Vianay, *Cell shape dynamics reveal balance of elasticity and contractility in peripheral arcs*, Biophys. J., 108 (2015), pp. 2437–2447, https://doi.org/10.1016/j.bpj.2015.04.005.

[28] M. Lenz, M. L. Gardel, and A. R. Dinner, *Requirements for contractility in disordered cytoskeletal bundles*, New J. Phys., 14 (2012), 33037, https://doi.org/10.1088/1367-2630/14/3/033037.

[29] M. P. Murrell and M. L. Gardel, *F-actin buckling coordinates contractility and severing in a biomimetic actomyosin cortex*, Proc. Natl. Acad. Sci. USA, 109 (2012), pp. 20820–20825, https://doi.org/10.1073/pnas.1214753109.

[30] P. Naumanen, P. Lappalainen, and P. Hotulainen, *Mechanisms of actin stress fibre assembly*, J. Microsc., 231 (2008), pp. 446–454, https://doi.org/10.1111/j.1365-2818.2008.02057.x.

[31] W. Nie, M. T. Wei, H. D. Ou-Yang, S. S. Jedlicka, and D. Vavylonis, *Formation of contractile networks and fibers in the medial cell cortex through myosin-*II *turnover, contraction, and stress-stabilization*, Cytoskeleton, 72 (2015), pp. 29–46, https://doi.org/10.1002/cm.21207.

[32] D. B. Oelz, B. Y. Rubinstein, and A. Mogilner, *A combination of actin treadmilling and cross-linking drives contraction of random actomyosin arrays*, Biophys. J., 109 (2015), pp. 1818–1829, https://doi.org/10.1016/j.bpj.2015.09.013.

[33] R. J. Pelham and F. Chang, *Actin dynamics in the contractile ring during cytokinesis in fission yeast*, Nature, 419 (2002), pp. 82–86, https://doi.org/10.1038/nature00999.

[34] L. J. Peterson, *Simultaneous stretching and contraction of stress fibers in vivo*, Mol. Biol. Cell, 15 (2004), pp. 3497–3508, https://doi.org/10.1091/mbc.E03-09-0696.

[35] T. D. Pollard, *Mechanics of cytokinesis in eukaryotes*, Curr. Opin. Cell Biol., 22 (2010), pp. 50–56, https://doi.org/10.1016/j.ceb.2009.11.010.

[36] T. D. Pollard, *Nine unanswered questions about cytokinesis*, J. Cell Biol., 216 (2017), pp. 3007–3016, https://doi.org/10.1083/jcb.201612068.

[37] M. Prager-Khoutorsky, A. Lichtenstein, R. Krishnan, K. Rajendran, A. Mayo, Z. Kam, B. Geiger, and A. D. Bershadsky, *Fibroblast polarization is a matrix-rigidity-dependent process controlled by focal adhesion mechanosensing*, Nat. Cell Biol., 13 (2011), pp. 1457–1465, https://doi.org/10.1038/ncb2370.

[38] P. Recho, T. Putelat, and L. Truskinovsky, *Contraction-driven cell motility*, Phys. Rev. Lett., 111 (2013), 108102, https://doi.org/10.1103/PhysRevLett.111.108102.

[39] B. Rubinstein, M. F. Fournier, K. Jacobson, A. B. Verkhovsky, and A. Mogilner, *Actin-myosin viscoelastic flow in the keratocyte lamellipod*, Biophys. J., 97 (2009), pp. 1853–1863, https://doi.org/10.1016/j.bpj.2009.07.020.

[40] M. S. Shutova, S. B. Asokan, S. Talwar, R. K. Assoian, J. E. Bear, and T. M. Svitkina, *Self-sorting of nonmuscle myosins* II*A and* II*B polarizes the cytoskeleton and modulates cell motility*, J. Cell Biol., 216 (2017), pp. 2877–2889, https://doi.org/10.1083/jcb.201705167.

[41] T. E. Sladewski, M. J. Previs, and M. Lord, *Regulation of fission yeast myosin-*II *function and contractile ring dynamics by regulatory light-chain and heavy-chain phosphorylation*, Mol. Biol. Cell, 20 (2009), pp. 3941–3952, https://doi.org/10.1091/mbc.E09-04-0346.

[42] J. R. Soiné, C. A. Brand, J. Stricker, P. W. Oakes, M. L. Gardel, and U. S. Schwarz, *Model-based traction force microscopy reveals differential tension in cellular actin bundles*, PLoS Comput. Biol., 11 (2015), pp. 1–16, https://doi.org/10.1371/journal.pcbi.1004076.

[43] M. R. Stachowiak, P. M. McCall, T. Thoresen, H. E. Balcioglu, L. Kasiewicz, M. L. Gardel, and B. O'Shaughnessy, *Self-organization of myosin* II *in reconstituted actomyosin bundles*, Biophys. J., 103 (2012), pp. 1265–1274, https://doi.org/10.1016/j.bpj.2012.08.028.

[44] M. R. Stachowiak and B. O'Shaughnessy, *Recoil after severing reveals stress fiber contraction mechanisms*, Biophys. J., 97 (2009), pp. 462–471, https://doi.org/10.1016/j.bpj.2009.04.051.

[45] M. R. Stachowiak, M. A. Smith, E. Blankman, L. M. Chapin, H. E. Balcioglu, S. Wang, M. C. Beckerle, and B. O'Shaughnessy, *A mechanical-biochemical feedback loop regulates remodeling in the actin cytoskeleton*, Proc. Natl. Acad. Sci. USA, 111 (2014), pp. 17528–17533, https://doi.org/10.1073/pnas.1417686111.

[46] S. X. Sun and S. Walcott, *Actin crosslinkers: Repairing the sense of touch*, Curr. Biol., 20 (2010), pp. R895–R896, https://doi.org/10.1016/j.cub.2010.08.059.

[47] T. Thoresen, M. Lenz, and M. L. Gardel, *Thick filament length and isoform composition determine self-organized contractile units in actomyosin bundles*, Biophys. J., 104 (2013),

pp. 655–665, https://doi.org/10.1016/j.bpj.2012.12.042.

[48] S. Tojkander, G. Gateva, A. Husain, R. Krishnan, and P. Lappalainen, *Generation of contractile actomyosin bundles depends on mechanosensitive actin filament assembly and disassembly*, eLife, 4 (2015), pp. 1–28, https://doi.org/10.7554/eLife.06126.001.

[49] S. Tojkander, G. Gateva, and P. Lappalainen, *Actin stress fibers - assembly, dynamics and biological roles*, J. Cell Sci., 125 (2012), pp. 1855–1864, https://doi.org/10.1242/jcs.098087.

[50] A. B. Verkhovsky, T. M. Svitkina, and G. G. Borisy, *Myosin* II *filament assemblies in the active lamella of fibroblasts: Their morphogenesis and role in the formation of actin filament bundles*, J. Cell Biol., 131 (1995), pp. 989–1002, https://doi.org/10.1083/jcb.131.4.989.

[51] S. Walcott and S. X. Sun, *Hysteresis in cross-bridge models of muscle*, Phys. Chem. Chem. Phys., 11 (2009), pp. 4871–4881, https://doi.org/10.1039/b900551j.

[52] S. Walcott and S. X. Sun, *A mechanical model of actin stress fiber formation and substrate elasticity sensing in adherent cells*, Proc. Natl. Acad. Sci. USA, 107 (2010), pp. 7757–7762, https://doi.org/10.1073/pnas.0912739107.

[53] S. Walcott and S. X. Sun, *Active force generation in cross-linked filament bundles without motor proteins*, Phys. Rev. E (3), 82 (2010), 050901(R), https://doi.org/10.1103/PhysRevE.82.050901.

[54] S. Walcott, D. M. Warshaw, and E. P. Debold, *Mechanical coupling between myosin molecules causes differences between ensemble and single-molecule measurements*, Biophys. J., 103 (2012), pp. 501–510, https://doi.org/10.1016/j.bpj.2012.06.031.

[55] Z. Zhou, E. L. Munteanu, J. He, T. Ursell, M. Bathe, K. C. Huang, and F. Chang, *The contractile ring coordinates curvature-dependent septum assembly during fission yeast cytokinesis*, Mol. Biol. Cell, 26 (2015), pp. 78–90, https://doi.org/10.1091/mbc.E14-10-1441.